Dynamics-based control of a one-legged hopping robot

S H Hyon[1]*, **T Emura**[1] and **T Mita**[2]
[1]Department of Mechatronics and Precision Engineering, Graduate School of Engineering, Tohoku University, Sendai, Japan
[2]Department of Mechanical and Control Engineering, Graduate School of Science and Engineering, Tokyo University, Tokyo, Japan

Abstract: This paper proposes a new model of a one-legged hopping robot. The one-legged hopping robot is useful in realizing rapid movement such as that of a running animal. Although it has a simple leg mechanism, the dynamics are not simple and require non-linear complex analysis. This means that it is not easy to derive a controller for stable hopping in a systematic way. Therefore, a dynamics-based approach was introduced where the controller is empirically derived based on characteristic dynamics. A prototype of the one-legged hopping robot was fabricated and a precise simulator of the robot, including actuator dynamics, was constructed to examine the usefulness of the proposed dynamics model. Applying the constructed simulator to the prototype, the robot succeeded in planar one-legged hopping.

Keywords: hopping robot, biomechanics, simulator, dynamics-based control

NOTATION

A_1, A_2	areas of cylinder chamber (m^2)
C_{ip}, C_{ep}	internal and external leakage coefficients (m^4 s/kg)
C_{tp}	total leakage coefficients (m^4 s/kg)
f_r, f_s	trajectory parameters for $\bar{r}$ and $\bar{\theta}$ (Hz)
F_f	friction force of cylinder (N)
F_L	load force of cylinder (N)
g	gravity constant (m/s^2)
i, i_1, i_2	constant current about vertical speed control (mA)
i_c	constant current about vertical speed control (mA)
K_1, K_2	feedback gain about position control for joints 1 and 2
K_f	feedback gain about forward speed control
K_i	current gain of servovalve
K_p	feedback gain about body pitch control
K_{static}	steady flow gain of servovalve
m_c	equivalent mass of cylinder piston, rod and oil (kg)
P_L	load pressure of servovalve (Pa)
P_s	supply pressure (Pa)
P_1, P_2	pressures of cylinder chamber (Pa)
q_1, q_2, q_3	joint angles (deg)
$\bar{q}_1$, $\bar{q}_2$	desired time trajectories of joints 1 and 2 (deg)
Q	output flow of servovalve (L/min)
Q_{in}/Q_{out}	flow into and out of cylinder (L/min)
Q_L	(dynamic) load flow of servovalve (L/min)
Q_{static}	static load flow of servovalve (L/min)
r	virtual leg length (m)
r_{max}	maximum virtual leg length (m)
r_{ret}	virtual leg length for retraction (m)
$\bar{r}$	desired time trajectory of virtual leg length at flight phase (m)
T_s	stance time (s)
V, V_1, V_2 V_{10}, V_{20}	volumes of cylinder chamber (m^3)
W_{in}, W_{out}	weight flowrates into and out of the servovalve
x	piston displacement in section 3, or hip position of robot in sections 4 and 5 (m)

The MS was received on 28 August 2002 and was accepted after revision for publication on 20 November 2002.
** Corresponding author: Department of Mechatronics and Precision Engineering, Graduate School of Engineering, Tohoku University, Aramaki-Aza-Aobo 01, Aobaku, Sendai 980-8579, Japan.*

x_a^2	desired forward speed (m/s)
z	vertical hip position (m)
z_a^2	desired vertical lift-off speed (m/s)
β_e	effective bulk modulus (Pa)
θ	damping coefficient of servovalve
θ_b	nominal touchdown angle of virtual leg (deg)
θ_f	desired touchdown angle of virtual leg (deg)
$\bar{\theta}$	desired time trajectory of virtual leg angle at flight phase (deg)
ρ, ρ_0	mass density of oil
ζ	damping coefficient of servovalve
ϕ	pitch angle of body (deg)
ϕ_d	desired body pitch angle (deg)
ω_n	natural frequency of servovalve (rad/s)

1 INTRODUCTION

In a gravity field, animals must bear ground force that is greater than twice their weight. Moreover, they receive a large impulse at touchdown. As many biomechanists have indicated, tendons play an important role in running or jumping motion. They store kinetic energy as potential energy during stance and also absorb the impulse at touchdown.

To realize a running robot, introducing such springy characteristics into leg design is quite natural. Pioneering work was done by Raibert and co-workers. They developed one-legged, biped and quadruped running robots; all of them had springy legs of the telescopic type and realized various running motions [**1**] (http://www.ai.mit.edu/projects/leglab/). Ahmadi and Buehler developed an electrically driven one-legged robot which had spring at the hip joint [**2**] and realized energy-efficient running using a modified Raibert controller [**3**] (http://www.cim.mcgill.ca/arlweb/).

Since Raibert's controller is based on uncontrolled dynamics of the springy leg, it does not require much control effort and yields a quite natural running gait. To embed uncontrolled dynamics into the control algorithm, Raibert made an assumption of decoupling of rotary motion of the body from telescopic motion of the leg. Therefore, for applying his controller to one-legged hopping, the mechanical model itself needs to be carefully designed to satisfy these assumptions: the leg should be sufficiently light compared to the body and the CM (centre of mass) of the body should be positioned closely to the hip joint.

Animal legs in nature, however, are of an articulated type; the CM of the body is set off the hip joint. As their dynamics have a strong non-linear coupling, analysis of uncontrolled dynamics is very difficult and there are few theoretical studies [**4**]; moreover, to the best of the authors' knowledge, there have been no successful experiments in hopping for this type of robot, except for two examples: Monopod [**5**] and Uniroo [**6**] studied by Raibert and co-workers. In order to realize robotic running copying that of animals, it is important to establish a general control method, but it is also important to invent several new mechanical models inspired by biology studies, such as the examples above, and to demonstrate successful experimental results. Success in experiments should be a great basis for developing a more sophisticated controller.

For this purpose, a new mechanical model of a dog hindlimb was proposed and a prototype of a one-legged hopping robot was designed as the first step towards the goal of dynamic quadruped running [**7**]. This robot has an articulated leg composed of three links; it uses two hydraulic actuators as muscles and linear springs as a tendon. However, the controller for hopping cannot be derived easily in a systematic (analytic) way because the robot has such complex non-linear dynamics. Therefore, as the first attempt, the controller was designed empirically based on the analysis of characteristic dynamics of the robot. To do this, a precise simulator including actuator dynamics was constructed.

In this paper, after describing the new leg model and hardware design of the robot, details of the simulator and the controller are presented. Using the dynamics-based controller, the robot has succeeded in producing planar one-legged hopping.

This paper is organized as follows. Section 2 describes the design and hardware of the one-legged hopping robot *Kenken*. Section 3 describes a precise simulator in which actuator dynamics are modelled in detail. Section 4 presents a dynamics-based controller for stable one-legged hopping. Section 5 gives results of simulation and experiment. Section 6 concludes the paper.

2 DEVELOPING THE ONE-LEGGED HOPPING ROBOT *KENKEN*

2.1 Proposal of a new mechanical model of the hindlimb

Alexander modelled a muscle and tendon system of a leg as a serial connection of inelastic actuator and a spring and studied the role of a tendon during running. In reference [**8**] he showed that a unique running speed exists where the length of muscle is maintained and mechanical energy is preserved. In this case, the mechanical work for running is not done by the muscle, but by the elastic tendon [**9**]. The Achilles tendon, in particular, is known to have large elasticity and the ability to store up to 35 per cent of mechanical energy in human or kangaroo running [**10**].

Assigning mechanical work only to the actuators is not an effective strategy for design of a robot capable of running, which needs more energy than walking. Instead, it is quite effective to use an energy storing mechanism like a spring. If doing so, the simplest and most direct implementation will be the linear mass–spring model adopted in Raibert's robots [**1**]. For studying the mechanism of animal running, this model is very tractable; also, many biomechanics researchers have dealt with this model. For example, McMahon and co-workers use this model to discuss the relationship between running speed and the spring constant in real animals [**11**, **12**].

However, there are some reasons why real animals adopt an articulated leg and not such a telescopic one. The practical advantages of an articulated-type leg can be summarized below:

1. Large reachability range → more clearance between the foot and ground.
2. Passive leg retraction during flight (provided if the link parameters are appropriately chosen).
3. Simple structure; it connects two ends of links with the rotary joint → easy construction.

In particular, advantage 2 is helpful for energy-efficient running and has already been seen in the passive walking robot [**13**].

There are several design solutions needed to make an articulated leg springy. Arranging the mechanism of serial connection of an inelastic actuator and a spring to each joint is one possibility. Using this design, Pratt and Pratt realized natural walking of a biped robot [**14**]. However, linkage of multiple passive joints with meaningful periodic running motion is such a difficult problem that there are no successful examples so far.

Instead of considering multiple passive joints, only the ankle joint was considered here because the largest tendons are at this joint. Figure 1 shows extensors of an ankle joint, which play the main role in running. Among them, this study specifically examined arrangement of the largest muscle groups, named gastrocnemius and plantaris. Then, the new leg model shown in Fig. 2 was proposed. It is a planar one-legged robot that has an articulated leg composed of three links. It has two active joints, the hip and knee, and one passive joint, the ankle;

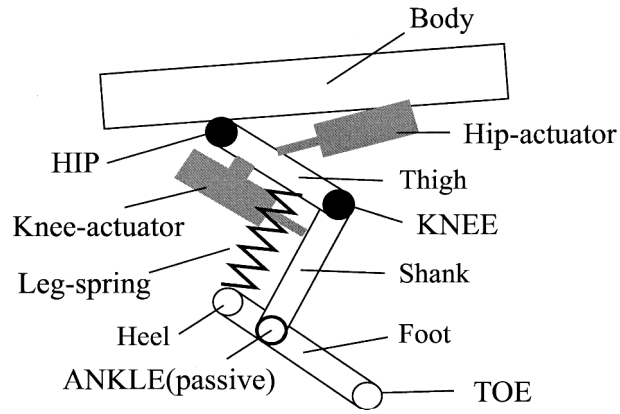

Fig. 2 One-legged robot with a new leg mechanism

there is no actuator at its foot (this means that the toe can rotate on the ground during the stance phase, acting as a free pivot).

The most distinctive feature of this model is the arrangement of the leg spring. The leg spring is attached between the thigh and heel parallel to the shank. Arrangement of the leg spring in this way creates the following two important effects during hopping:

1. During stance, holding the knee joint enables the leg spring to absorb a large impulse at touchdown and to transfer its kinetic energy to potential energy for the next stride. Extending the knee yields an extra displacement of the spring; hence it adds potential energy to the spring (Fig. 3).
2. During flight, the spring constitutes a member of the 'parallel four-bar linkage' because compressive force to the spring is not so large at that duration. Consequently, it enables passive retraction and extension of the leg, provided the inertia of the links is chosen appropriately (Fig. 4).

Prilutsky *et al.* show by experiments with cats that there is a transfer of energy between the ankle and knee joints via the gastrocnemius and plantaris; they conclude that this facilitates an energy-efficient running motion [**15**]. This model elucidates how the ankle tendon operates on the run, in combination with proximal joint motions. On the other hand, the spring arrangement in *Uniroo* [**6**] is the same as the soleus in Fig. 1.

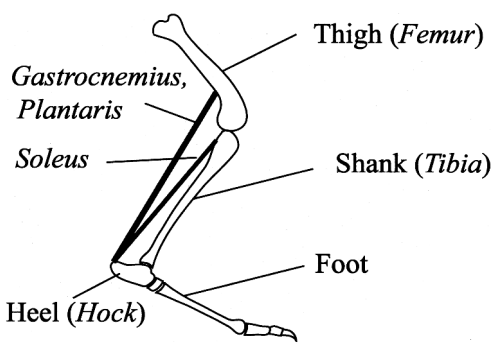

Fig. 1 Extensor muscle groups of the ankle joint

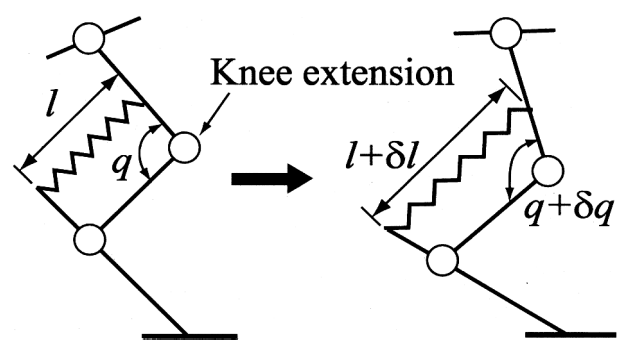

Fig. 3 Active energy pumping

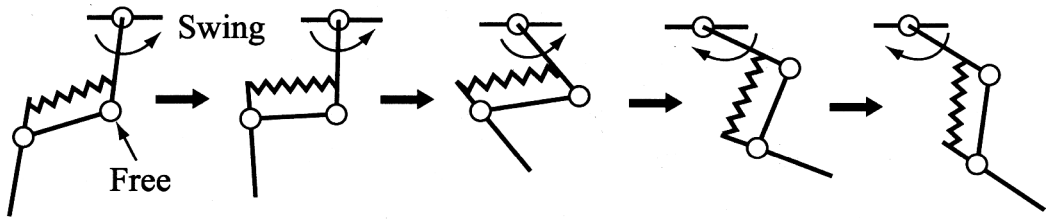

Fig. 4 Passive leg retraction

Figure 5 illustrates one stride of the hopping motion, together with each instant of phase transition (touchdown, bottom, lift-off, apex).

2.2 Hardware overview

Figure 6 shows Kenken, the prototype one-legged hopping robot that realized the leg model proposed in the previous section. The main specifications are given in Table 1.

A medium-sized dog of about 0.5 m in hip height was selected as a target model. A length of all links (including a foot) was chosen to be the same, 0.18 m, for tractability of the kinematics. This corresponds to the range of the leg length from 0.31 to 0.54 m for ideal parallel four-bar linkage. The mass of the leg is relatively large, 3.6 kg. Individual masses of thigh, shank and foot are 2.42, 0.75 and 0.43 kg respectively. The CM offset from the hip joint is about 0.10 m. For the leg spring, two tensile coil springs are installed in parallel between the thigh and heel. The initial value of the spring constant was determined by simple energy analysis.

Since running requires relatively high energy and always accompanies shock against the ground, joint actuation is the most critical problem for hardware

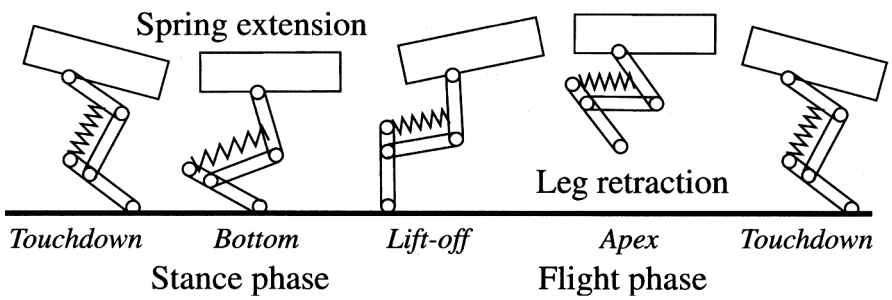

Fig. 5 Illustration of one hopping stride

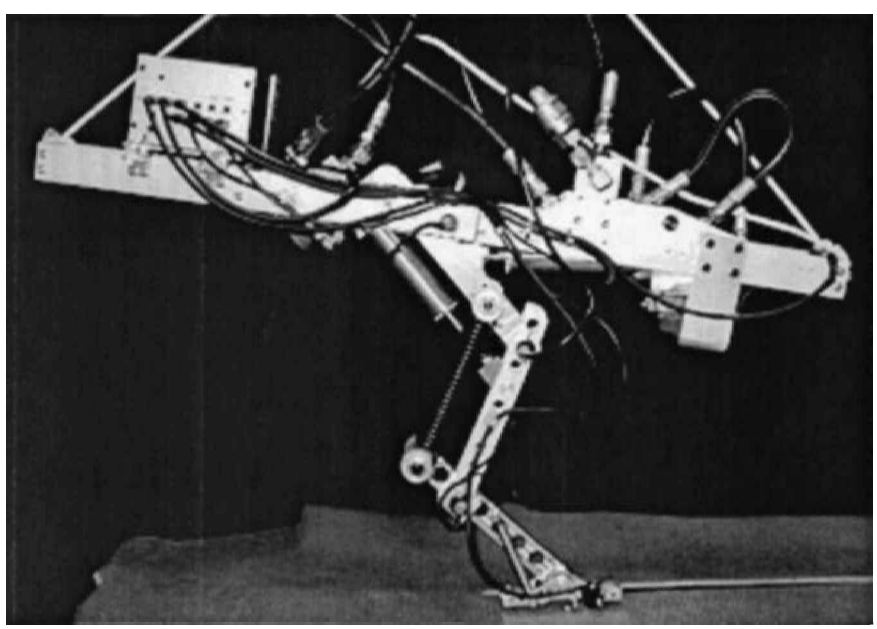

Fig. 6 One-legged hopping robot—Kenken

Table 1 Main specifications of Kenken

Parameter	Unit	Value
Total mass	kg	13.26
Body mass (including boom)	kg	9.66 (0.5)
Leg mass	kg	3.60
Body length	m	0.85
Thigh, shank, foot length	m	0.18
Toe length	m	0.05
Leg length (maximum)	m	0.52
Leg length (minimum)	m	0.31
Maximum stride	m	0.52
Body inertia around hip	kg m^2	0.46
Leg inertia around hip (maximum)	kg m^2	0.13
Leg inertia around hip (minimum)	kg m^2	0.07
Leg spring coefficient (each)	N/m	10 000
Length of moment arm	m	0.06
Rated actuator force at 14 MPa	N	2200
Rated actuator speed at 14 MPa	m/s	2.21

realization. Therefore, the authors introduced powerful hydraulics and developed a small lightweight servo-actuator, directly mounted with an industry servovalve (Fig. 7). In this sense, the authors gave priority to stiffness over autonomy. The actuator force must be zero for the passive leg retraction during flight, mentioned in section 2.1. However, this is difficult for a commercial flow-control servovalve; it was abandoned at the prototype stage.

The experimental set-up is similar to that of Raibert. A tether boom constrains the robot to the sagittal plane and measures the horizontal position, vertical position and pitch angle of the body via three optical encoders. It also carries hydraulic hoses, a signal line and a d.c. line. An aluminium box attached to the rear includes an interface circuit, servo-amplifier and signal conditioning circuit, which were hand-made taking the impulses and vibrations into account. The control program is written in MATLAB/SIMULINK code and runs in a single timer task with a 0.5 ms sampling period.

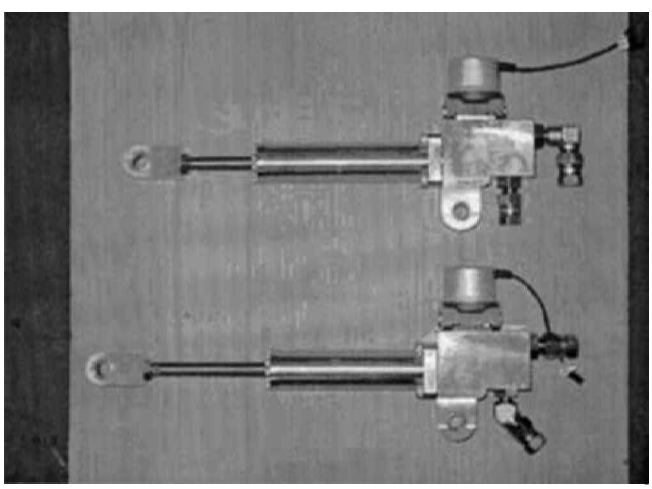

Fig. 7 Hydraulic servo-actuator of Kenken

3 BUILDING A PRECISE SIMULATOR

It is difficult to derive the controller in a systematic way because the robot has the quite complex non-linear dynamics described below.

1. Under-actuated sytem. The robot has an articulated leg with a passive joint. It has no actuator at its sole.
2. Hybrid system. The dynamics of the robot change drastically while the robot transits through to a stance phase, flight phase, touchdown, etc.
3. Periodic system. Linearization around equilibrium points and stabilization has no meaning; instead, their orbital stability is needed.

Therefore, as the first attempt, the controller was designed empirically based on analysis of the characteristic dynamics of the robot. A precise simulator was constructed for this purpose.

MATLAB-based graphical programming was introduced for flexibility and rapid prototyping of the controller. Specifically, the mechanical model of the robot and contact model with the ground was constructed using DADS; also, the hydraulic actuator was modelled as a general electrohydraulic system using SIMULINK. Figure 8 shows a block diagram of the simulator. The dashed line indicates the simulation model described below. If the simulation model is replaced by an actual mechanical model through the sensor input/output interface, the controllers developed and estimated on the simulator can be applied immediately to the actual robot.

3.1 Modelling of a link system

The link model of the robot was constructed with DADS, which enables graphical modelling of the mechanical system while simplifying dynamic motion simulation. Its interior mechanism is not a 'black box' but is based on Haug's book [**16**] and is easy to follow.

Mechanical parts are modelled as simple rigid links having actual robot parameters. Although Kenken is a planar hopping robot, it moves in constrained three-dimensional space. Therefore, a three-dimensional model was used; a tether boom was also modelled as in the experimental set-up.

A contact model is realized as a point-segment contact element of DADS, which was set between the tip of the sole and ground, where Young's modulus, the friction coeffcient and the restitution coefficient are set appropriately. For contact modelling details, see the paper of Haug *et al.* [**17**].

3.2 Modelling of a hydraulic servosystem

The actuating system of Kenken is a typical electro-hydraulic servosystem shown in Fig. 9. As mentioned

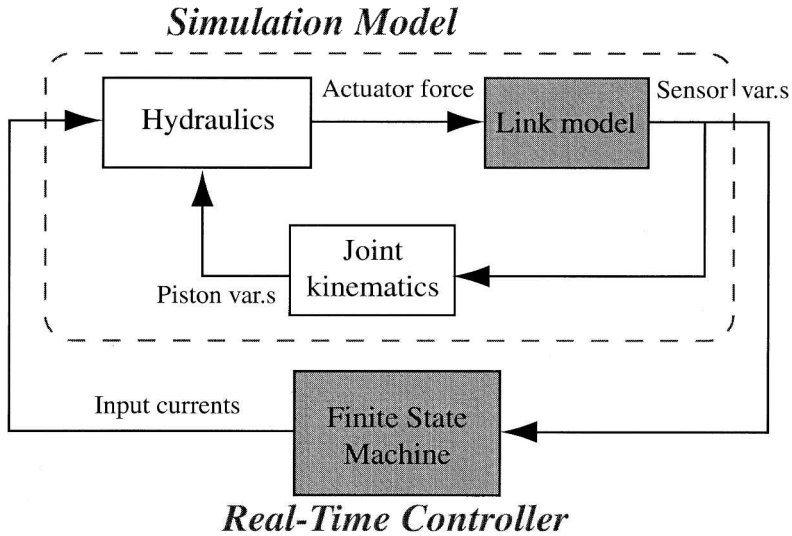

Fig. 8 Block diagram of a simulator

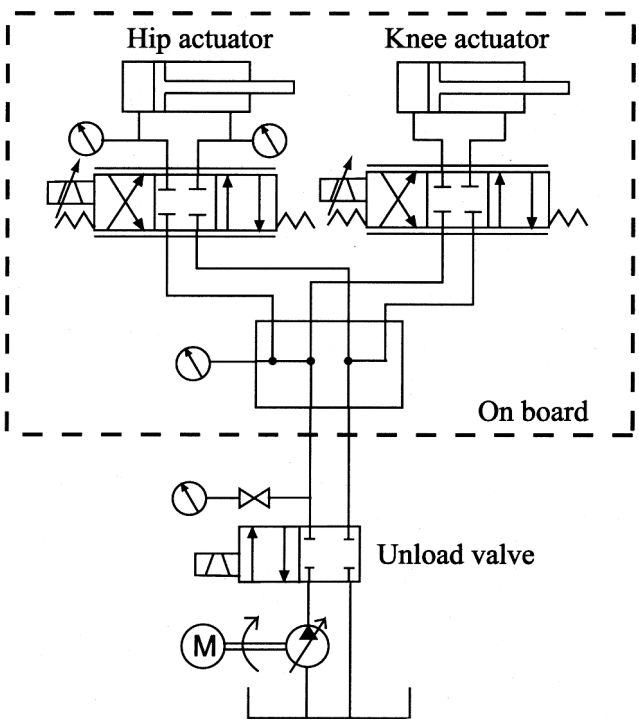

Fig. 9 Hydraulic system

before, the controller is derived based on the characteristic dynamics. The most important dynamics are 'uncontrolled' (or 'passive') dynamics, which means that the dynamics appear when applied torques are set to zero. This is, however, a problem for the present robot because a flow-controlled hydraulic servo-actuator has less force controllability (the active joints are very stiff). (The authors refer readers to reference [**18**] for the force control using a flow-controlled hydraulic servovalve. Reference [**19**] should also be referred to, where an interesting force controllable actuator composed of a spring and hydraulic actuator in series is described.) Therefore, the control input is defined as the input currents to the servo-amplifier, instead of the actuator force. If doing so, actuator dynamics exert a large influence on the total dynamics of the robot. In this way, a sufficiently precise model of the actuator was built.

3.2.1 *Servovalve dynamics*

Dynamic characteristics of the servovalve are given as the transfer function for input current i to output flow Q:

$$\frac{Q(s)}{i(s)} = \frac{K_{\text{static}}\omega_{\text{n}}^2}{s^2 + 2\zeta\omega_{\text{n}}s + \omega_{\text{n}}^2} \tag{1}$$

where ω_{n} and ζ are the natural frequency and damping coefficients of the servovalve respectively and K_{static} is the static gain. On the other hand, for a given pressure supply P_{s} and load pressure P_{L}, the static load flow Q_{static} is written as

$$Q_{\text{static}} = K_i\sqrt{P_{\text{s}} - \text{sign}(i)P_{\text{L}}} \tag{2}$$

where K_i is the current gain.

These equations can be combined in the block diagram of Fig. 10. This system calculates the (dynamic) load flow Q_{L} for a given input current i and load pressure P_{L}. Note that the dynamic part of the servovalve [equation (1)] is implemented as a current filter. All the servovalve parameters can be obtained from the catalogue [**20**].

3.2.2 *Continuity equation of hydraulic flow*

The continuity equation for the cylinder is written as

$$W_{\text{in}} - W_{\text{out}} = g\rho\frac{\text{d}V}{\text{d}t} + gV\frac{\rho}{\beta_{\text{e}}}\frac{\text{d}P}{\text{d}t} \tag{3}$$

where W represents the weight flowrates into and out of a valve, g is a gravity constant, ρ is the mass density, V is the volume of the chamber and β_{e} is the effective

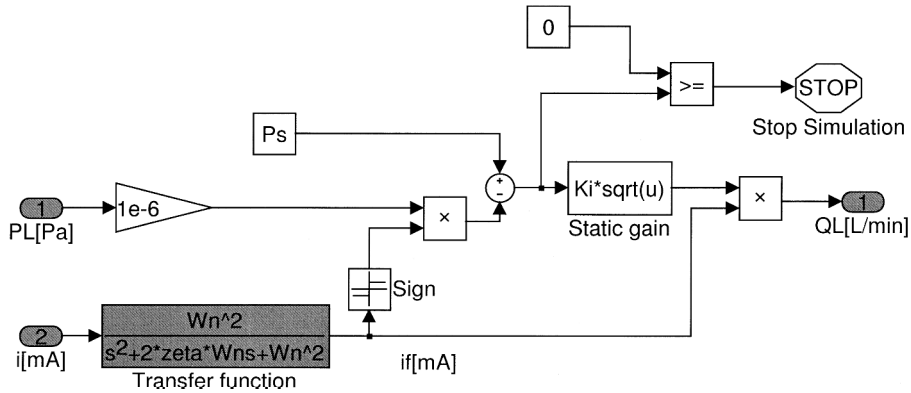

Fig. 10 Servovalve dynamics

bulk modulus [**21**]. In general, ρ is a function of temperature and pressure; however, if temperature is supposed to be constant during experimentation, ρ is expressed as a linear function of pressure:

$$\rho = \rho_0 + \frac{\rho_0}{\beta_e} P \tag{4}$$

where ρ_0 is the initial value. Considering that $W = g\rho Q$ yields

$$Q_{in} - Q_{out} = \frac{dV}{dt} + \frac{V}{\beta_e} V \frac{dP}{dt} \tag{5}$$

where the quadratic term of ρ is neglected.

For the cylinder of Fig. 11, the load flow Q_L becomes

$$\begin{aligned} Q_L &= \frac{1}{2}(Q_1 + Q_2) \\ &= \frac{1}{2}\left[C_{ip}(P_1 - P_2) + C_{ep}P_1 + \frac{dV_1}{dt} + \frac{V_1}{\beta_e} V_1 \frac{dP_1}{dt} \right] \\ &\quad + \frac{1}{2}\left[C_{ip}(P_1 - P_2) - C_{ep}P_2 - \frac{dV_2}{dt} - \frac{V_2}{\beta_e} V_2 \frac{dP_2}{dt} \right] \end{aligned} \tag{6}$$

where C_{ip} and C_{ep} are the internal leakage coefficient and external leakage coefficient. Using piston displacement x, the volumes of each chamber are written as

$$V_1 = V_{10} + A_1 x \tag{7}$$

$$V_2 = V_{20} - A_2 x \tag{8}$$

where V_{10} and V_{20} are initial volumes. On the other hand,

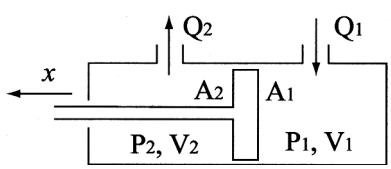

Fig. 11 Single-ended cylinder: x is the piston displacement, A_1, A_2 are piston areas, V_1, V_2 are volumes, P_1, P_2 are pressures and Q_1, Q_2 are flowrates of each chamber

using the load pressure P_L, the pressures of each chamber can be written as

$$P_1 = \frac{P_s + P_L}{2} \tag{9}$$

$$P_2 = \frac{P_s - P_L}{2} \tag{10}$$

Substituting equations (7) to (10) into equation (6), the relationship between the load flow and load pressure becomes

$$\begin{aligned} Q_L &= \frac{1}{2}(A_1 + A_2)\dot{x} + C_{tp}P_L \\ &\quad + \frac{1}{4\beta_e}[V_{10} + V_{20} + (A_1 - A_2)x]\dot{P}_L \end{aligned} \tag{11}$$

where $C_{tp} = C_{ip} + C_{ep}/2$ are the total leakage coefficients. This equation represents hydraulic compressibility and is expressed by the block diagram in Fig. 12.

3.2.3 *Equation of motion for cylinder dynamics*

Let m_e be the equivalent mass of the cylinder piston, rod and hydraulic oil. The equation of motion for the cylinder becomes

$$m_e\ddot{x} + F_f + F_L = A_1P_1 - A_2P_2 \tag{12}$$

or, using equations (9) and (10),

$$m_e\ddot{x} + F_f + F_L = \frac{P_s}{2}(A_1 - A_2) + \frac{P_L}{2}(A_1 + A_2) \tag{13}$$

where F_f is the friction of the cylinder and F_L is the load.

3.2.4 *Total system*

The above subdynamics are combined to obtain Fig. 13. A given input current and cylinder rod position and velocity gives the cylinder force. Parameters of the servovalve are borrowed from reference [**20**]. Some constants are obtained from identification tests in section 3.3.

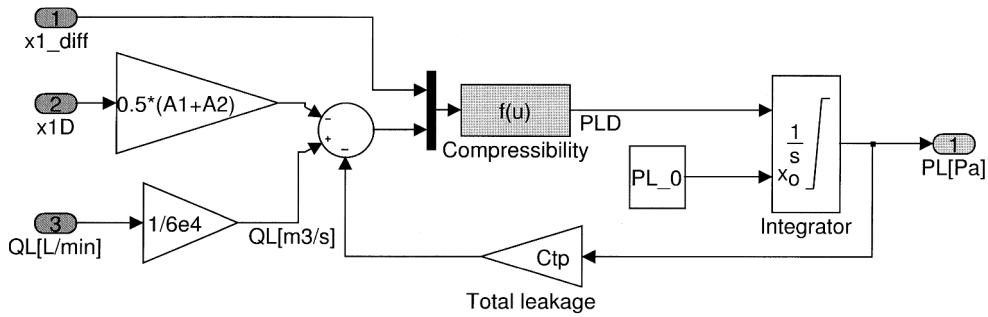

Fig. 12 Hydraulic compressibility

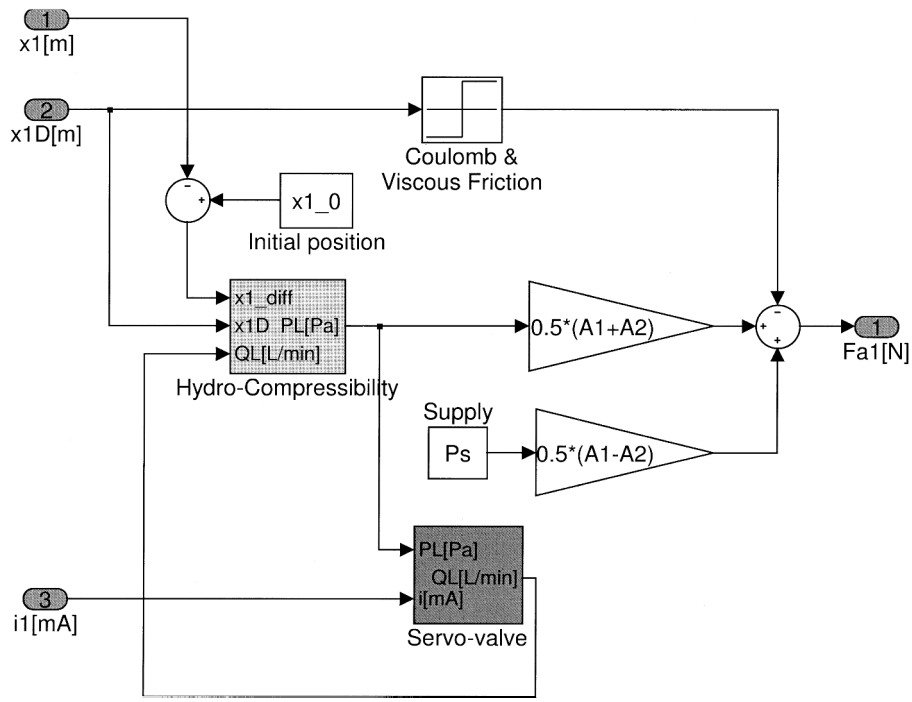

Fig. 13 Block diagram of the servo-actuator (hip actuator only)

3.3 Actuator identification

Due to the piston seal and other elements, the hydraulic actuator has a relatively large friction. It is not realistic to ignore the friction term. The simple method used to identify friction in reference [**18**] is used. Rearranging equation (12) gives

$$\hat{F}_{\mathrm{f}} = A_1 P_1 - A_2 P_2 - F_{\mathrm{L}} - m\ddot{x} \tag{14}$$

where $\hat{}$ denotes an ideal value. If pressure, acceleration and load are known exactly, friction can be identified. Other parameters, such as β_{e} and C_{tp}, were identified using the least-squares method.

Figure 14 shows the results of simulation and an experiment of a driving test (tracking to a sinusoidal curve) after identification. This figure shows that the actuator dynamics is sufficiently and precisely modelled on the simulator.

4 DYNAMICS-BASED CONTROLLER FOR STABLE HOPPING

In this section, the controller for stable hopping is derived based on the basic characteristic dynamics of the robot. The controller is in the form of a finite state machine (FSM); i.e. one hopping stride is divided into several discrete states. Then, the transition (switching) rule and the control law for each state are derived. The continuous states of the system transit according to this FSM. If the controllers and parameters are well chosen, periodic hopping gaits are expected to appear.

The coordinates of the robot are defined in Fig. 15.

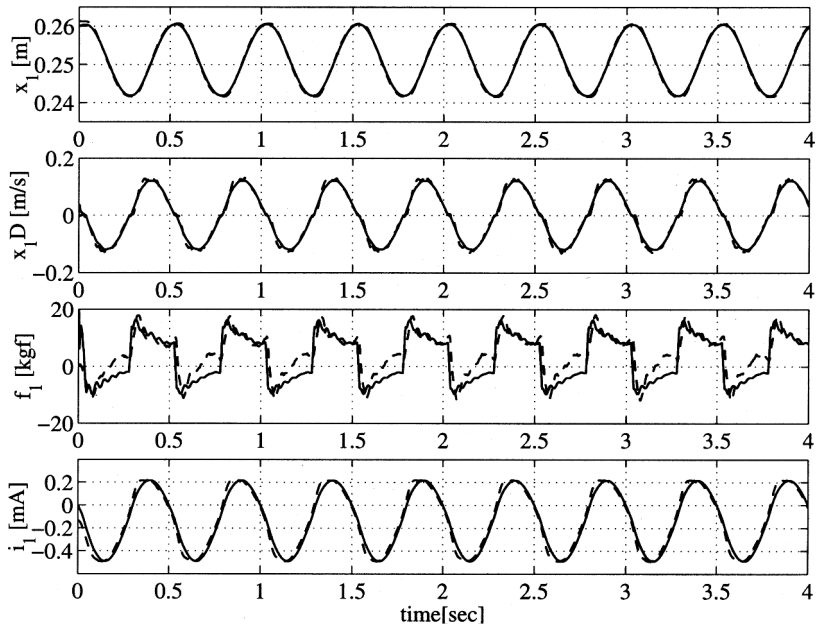

Fig. 14 Simulation results (solid line) and experimental results (dashed line) of a load driving test of the servo-actuator: x_1 is piston displacement, x_1D is piston velocity, f_1 means applied force and i_1 is input current

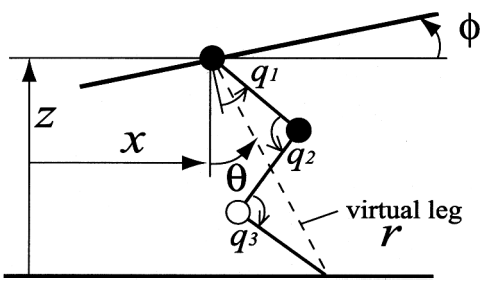

Fig. 15 Coordinates (● denotes actuated joints, ○ denotes the passive joint)

The controlled variables are $(\dot{x}, \dot{z}, \dot{\phi})$: the forward speed, vertical speed and attitude of the body in the sagittal plane. The virtual leg length r and angle θ, which are used in the control at flight, are also defined in the figure. Control inputs i_1 and i_2, the input currents to the hip actuator and the knee actuator respectively.

Below, characteristic dynamics of the simulated robot are explored in section 4.1. Then, the control law for the stance phase and flight phase are developed in sections 4.2 and 4.3 respectively. They are combined with the FSM in section 4.4.

4.1 Characteristic dynamics of the model

Using the precise simulator developed in section 3, characteristic dynamics are explored.

Firstly, passive dynamics of free fall are investigated. The robot is set to the nominal configuration in which the foot is below the CM, and both control inputs are set to zero ($i_1 = 0$, $i_2 = 0$). Then, the following behaviour was observed (Fig. 16):

(a) At the instant of touchdown, a large impulsive ground force makes the body pitch forward suddenly.
(b) From touchdown to the bottom, the body pitches forward ($\dot{\phi} < 0$) because of the negative reaction moment.
(c) After maximum extension of the leg spring, the body pitches backward ($\dot{\phi} > 0$).
(d) When the vertical reaction force becomes zero, the robot lifts off with positive angular momentum.

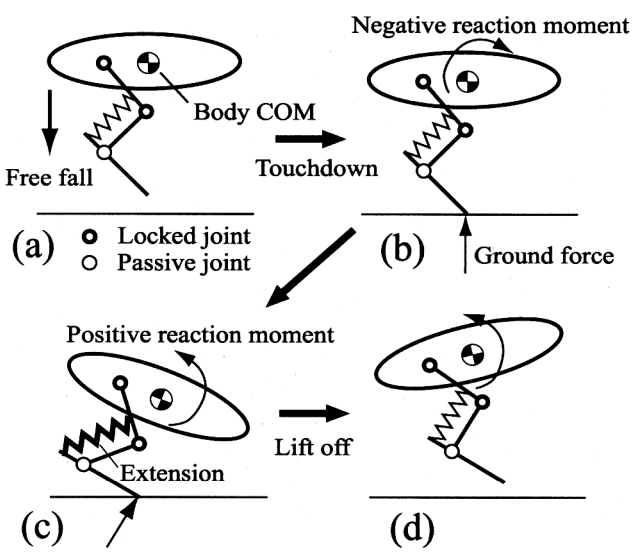

Fig. 16 Passive motion

Whether it lifts off forward or backward depends on the foot placement at touchdown. This fact is utilized in the forward speed control in section 4.3.

Next, actuated dynamics were investigated because these are the basis for control actions, which are selected according to the system state. Here, the robot is set to the nominal configuration, with its foot contacting the ground. Then, the constant inputs are fed to one actuator (Fig. 17):

(e) If extending the hip actuator with the knee fixed ($i_1 > 0$ and $i_2 = 0$), the leg spring is extended and backward body pitching ($\dot{\phi} > 0$) occurs.
(f) If extending the knee actuator with the hip fixed ($i_2 > 0$ and $i_1 = 0$), the leg sring is extended and forward body pitching ($\dot{\phi} < 0$) occurs.
(g) If shortening the hip actuator with the knee fixed ($i_1 < 0$ and $i_2 = 0$), the spring buckles (of course this is not allowed).
(h) If shortening the knee actuator with the hip fixed ($i_2 < 0$ and $i_1 = 0$), undesirable oscillation and chattering occurs.

Although there are some quantitative differences from the initial configuration and the amount of the inputs, the qualitative behaviour is identical.

4.2 Control during the stance phase

Since the robot has only two inputs, three coordinates cannot be controlled independently. Based on observations of the characteristic dynamics above, the attitude and the vertical speed of the body are controlled as follows during the stance phase:

$$i_1 = \begin{cases} -K_p(\phi - \phi_d), & \text{if } \phi \leqslant \phi_d \\ 0, & \text{else} \end{cases} \tag{15}$$

$$i_2 = \begin{cases} i_c, & \text{if } \dot{q}_3 \geqslant 0,\ \dot{z} \leqslant \dot{z}_d,\ r < r_{max} \\ 0, & \text{else} \end{cases} \tag{16}$$

where K_p is a position gain, ϕ_d is a desired attitude, $\dot{z}_d$ is a desired vertical speed, i_c is a constant current and r_{max} is the maximal virtual leg length.

Equations (15) and (16) mean that the hip actuator controls body pitch by a feedback law, which is executed 'only when' the pitch angle is lower than a specified value, while the knee actuator controls vertical speed and also suppresses the backward body pitch by giving a constant input, which is exerted 'only when' maximum spring extension occurs.

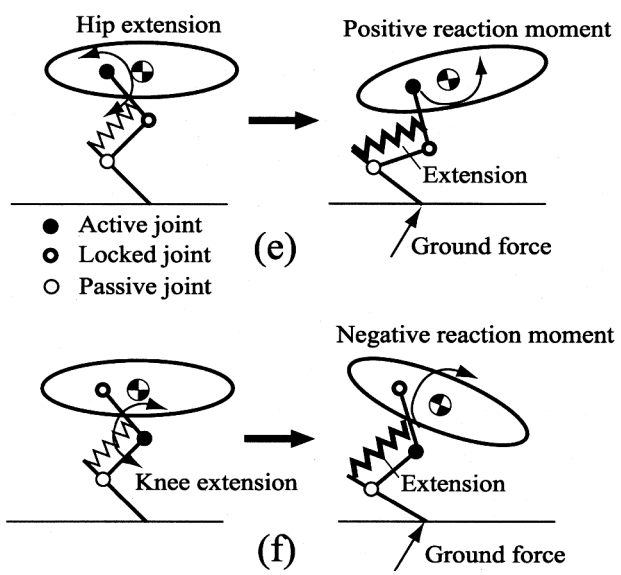

Fig. 17 Actuated motion

4.3 Control during the flight phase

During flight, the robot swings the leg to prepare for the next touchdown. It also retracts and extends the leg to reduce inertia for fast leg swinging and prevent stubbing against the ground. Note that the touchdown angle (foot placement) of the leg is critical to gait stability for robots that cannot change their leg lengths arbitrarily and have no actuator at their foot [**22**].

Although Kenken has no actuator at its foot, it has a knee actuator that can be used to control its leg length. However, the knee actuator has already been used for vertical speed control. Hence, the touchdown leg angle was used for forward speed control, following Raibert's algorithm [**1**].

In other words, the desired touchdown angle θ_f of the virtual leg is chosen as

$$\theta_f = \theta^* + K_f(\dot{x} - \dot{x}_d) + \theta_b \tag{17}$$

where

$$\theta^* = \arcsin\left(\frac{1}{r_0}\frac{\dot{x}T_s}{2}\right) \tag{18}$$

Here $\dot{x}_d$ is a desired forward speed and T_s is the stance time, which decreases as the forward speed increases [**12**]. The constant r_0 is the nominal length of the virtual leg and θ_b is a nominal bias term introduced empirically to reduce coupling effects from the offset of the CM. Control parameters are the feedback gain K_f and θ_b.

Having determined the touchdown angle θ_f, the hip actuator swings the leg so that it tracks a smooth reference trajectory $\overline{\theta(t)}$, which reaches θ_f (Fig. 18, upper). Also, for leg retraction, a smooth reference trajectory $\overline{r(t)}$, which reaches the nominal length r_0 (Fig. 18,

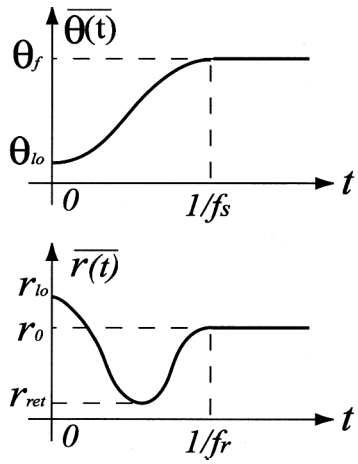

Fig. 18 Reference trajectories of θ and r during flight

below), was given. Specifically, the robot tracks the path

$$\overline{\theta(t)} = \frac{\theta_{lo} + \theta_f}{2} + \frac{\theta_{lo} - \theta_f}{2}\cos(2\pi f_s t) \tag{19}$$

$$\overline{r(t)} = \frac{r_{lo} + r_{ret}}{2} + \frac{r_{lo} - r_{ret}}{2}\cos(2\pi f_r t) - (r_{lo} - r_0)(1 - f_r t) \tag{20}$$

where t is the time after lift-off, r_{lo} is the leg length at lift-off, r_{ret} is the leg length of retraction, θ_{lo} is the lift-off angle and f_r and f_s determine the speed of convergence. They are chosen large enough to complete swing and retraction.

Then, the simple local feedback law can be applied:

$$i_1 = -K_1(q_1 - \overline{q_1}) \tag{21}$$

$$i_2 = -K_2(q_2 - \overline{q_2}) \tag{22}$$

In these equations, $\overline{q_1} = q_1(\overline{r(t)}, \overline{\theta(t)})$, $\overline{q_2} = q_2(\overline{r(t)}, \overline{\theta(t)})$ are the desired joint trajectories calculated via inverse kinematics of the parallel four-bar linkage mechanism and K_1, K_2 are the position gains.

4.4 Implementation of the controller

Figure 19 shows the FSM, which combines the controllers described in sections 4.2 and 4.3. Each discrete state and the corresponding control law, as well as events and corresponding switching conditions, are summarized in Table 2, where sw represents the on/off state of the foot switch. A situation that does not obey these transition rules implies falling down.

5 SIMULATIONS AND EXPERIMENTS

Hopping simulations and experiments were carried out using the controller derived in the previous section. Table 3 shows the initial conditions and control parameters used in both the simulation and experiments. These parameters were partially tuned on the simulator and then applied to the experiments. Since optimization or learning control had not yet been applied, the control parameters were tuned by hand.

Firstly, the simulation results are shown. The robot is initially set to be 0.1 m away from the ground; it is then dropped. Figure 20 shows snapshots of animation during hopping when the desired forward speed $\dot{x}_d$ was set to 1 m/s. Two arrows running from the sole represent the ground reaction forces.

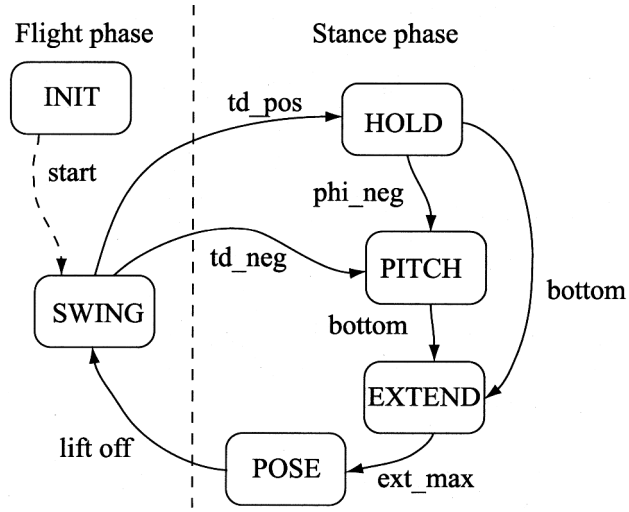

Fig. 19 Finite state machine

Table 2 Details of events and control actions

State	Control action
HOLD	$i_1 = 0$, $i_2 = 0$
PITCH	$i_1 = -K_p(\phi - \phi_d)$, $i_2 = 0$
EXTEND	$i_1 = -K_p(\phi - \phi_d)$ or 0, $i_2 = i_c$
POSE	$i_1 = 0$, $i_2 = 0$
SWING	$i_j = -K_j(q_j - \overline{q_j})$ $(j = 1, 2)$
Event	**Condition when event occurs**
td_pos	$sw = 1$, $\phi - \phi_d > 0$
td_neg	$sw = 1$, $\phi - \phi_d \leqslant 0$
phi_neg	$\phi - \phi_d \leqslant 0$
bottom	$\dot{q}_3 \geqslant 0$
ext_max	$r = r_{max}$ or $z - z_d > 0$
lift off	$sw = 0$

Table 3 Initial conditions and control parameters: during experiments, only the desired forward speed $\dot{x}_d$ is varied

	Unit	Value		Unit	Value
ϕ_0	deg	−10	K_p	mA/rad	7
θ_0	deg	10	i_c	mA	0.5
r_0	m	0.47	K_f	s/m	0.1
z_0	m	0.55	θ_b	deg	10
θ_d	deg	−5	K_1	mA/rad	100
$\dot{z}_d$	m/s	2	K_2	mA/rad	100

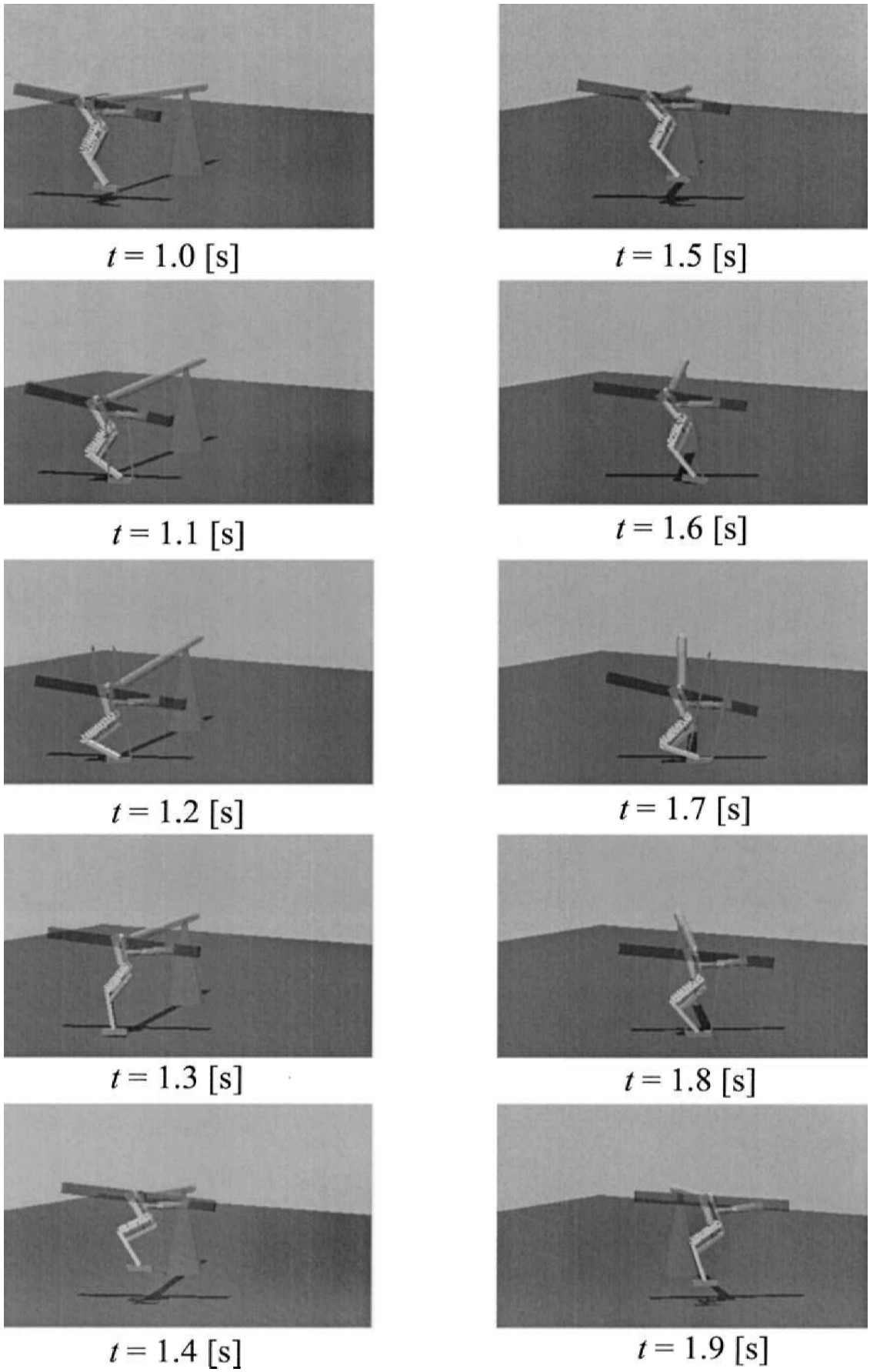

Fig. 20 Snapshots of DADS animation

Figure 21 depicts time evolutions of each state. Note that $\dot{x}$ (denoted by XD in the figures) represents the velocity of the hip, not of the CM. Foot SW represents the state of the foot switch. The dashed line in the graph of r and θ represents a 'dummy' trajectory, i.e. a situation where the angles of the ankle and knee are the same ($q_3 = q_2$).

Next, experimental results with the same conditions are shown in Fig. 22. Compared with Fig. 21, time evolutions of each state are similar to those of the simulation. After four steps, the forward speed $\dot{x}$ converges to the desired value of 1 m/s. The hopping period is about 0.5 s. The pitch angle ϕ is oscillating within 0° to -15°, which means that the robot is stable. The two control inputs, i_1 and i_2, also shift similarly, which means that the variation of hydraulic pressure in the simulation and the experiment are almost identical.

However, some differences were found. One is the small difference in transition, which is not so important for control tasks. This comes from an unavoidable gap of initial conditions in the experiment. Another difference is the hopping height. In experiments, the hopping height converged to a larger value than in the simulation. It is supposed that the difference arose from the control law [equation (16)], which is described in the form of feedforward. Therefore, it should be more able to control vertical speed in the form of global feedback as in equation (17).

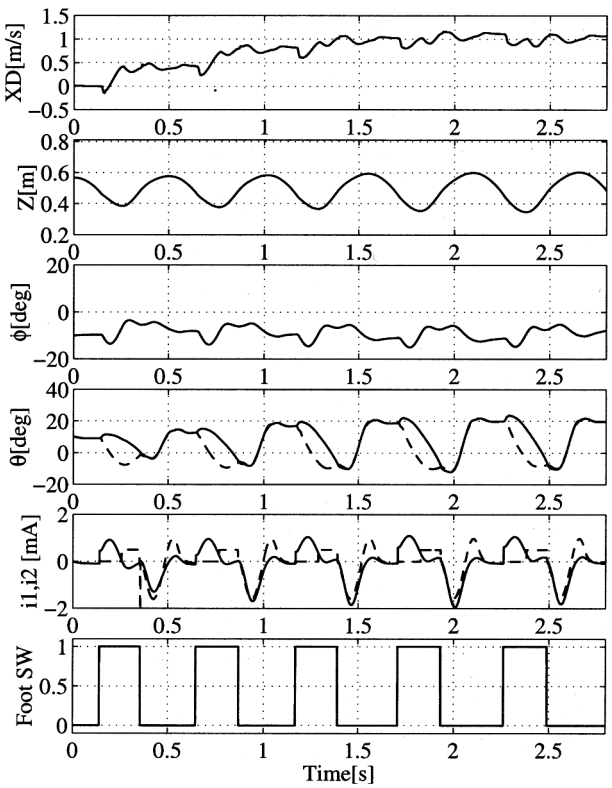

Fig. 21 Simulation results when $\dot{x}_d = 1.0$

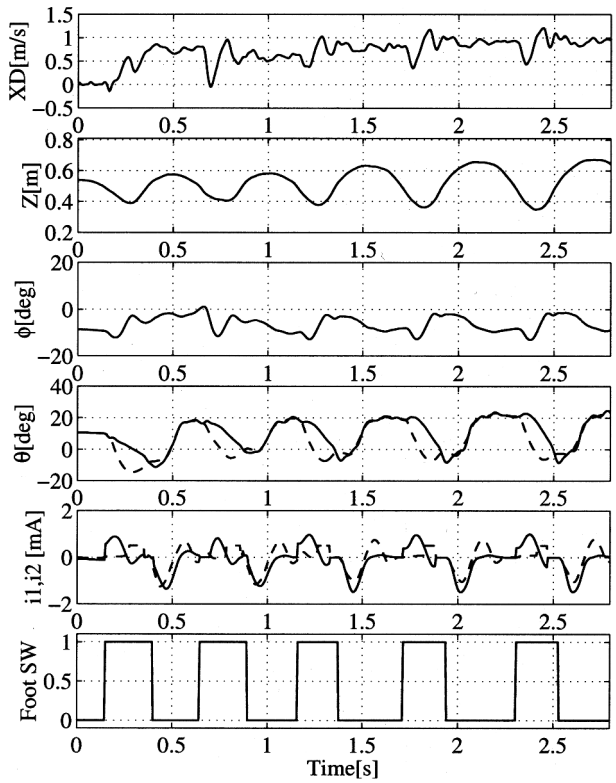

Fig. 22 Experimental results when $\dot{x}_d = 1.0$

Experiments were also carried out for various desired forward speeds. For example, Figs 23 and 24 show results for low-speed ($\dot{x}_d = 0.5$ m/s) and high-speed hopping ($\dot{x}_d = 1.5$ m/s). It is found that the robot can hop stably at speeds below 1 m/s, including vertical hopping, in both simulation and experiment. In this case, pitch angles oscillate around relatively higher values. However, at speeds over 1.5 m/s, stability deteriorates. Specifically, the forward and vertical speed and body pitch angle oscillate drastically. It is still stable, but tracking to a specific speed becomes difficult. Moreover, once forward speed exceeds 2 m/s, the leg angle easily reaches the limit of the movable range and it becomes impossible to retain gait stability.

Instability at higher speeds is related to speed-dependent deviations of the pitch angle at touchdown. The faster the desired speed, the larger the leg angle at touchdown because of equation (17), which results in more nose-down body pitch angle at touchdown. Then, the large error of the pitch angle turns to the large hip torque and propels the robot strongly during stance. This process causes the system to diverge.

There are two ways to avoid such a deviation of the body pitch angle at touchdown. The simplest way is to replace the leg by a less massive one. This reduces the amplitude of body pitching relative to leg swinging during the flight phase. The other way is to actively control body pitching by installing a tail mechanism into

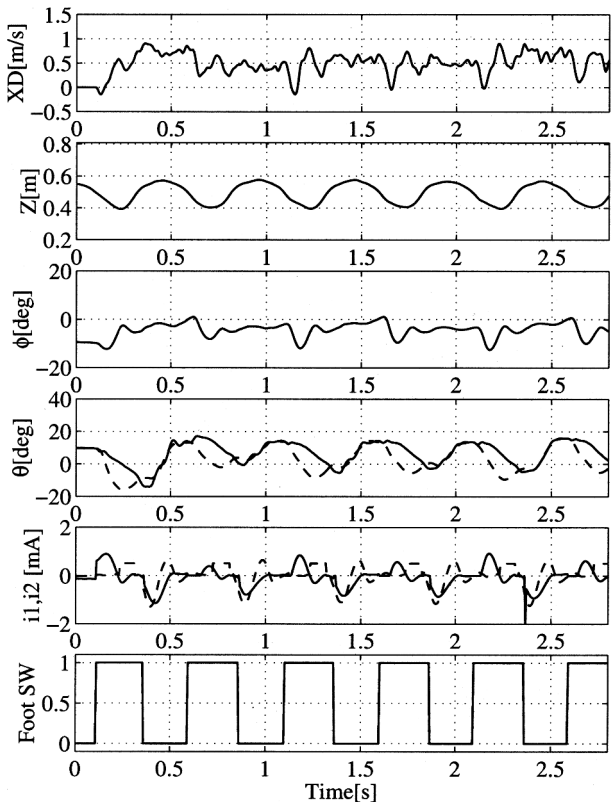

Fig. 23 Experimental results when $\dot{x}_d = 0.5$

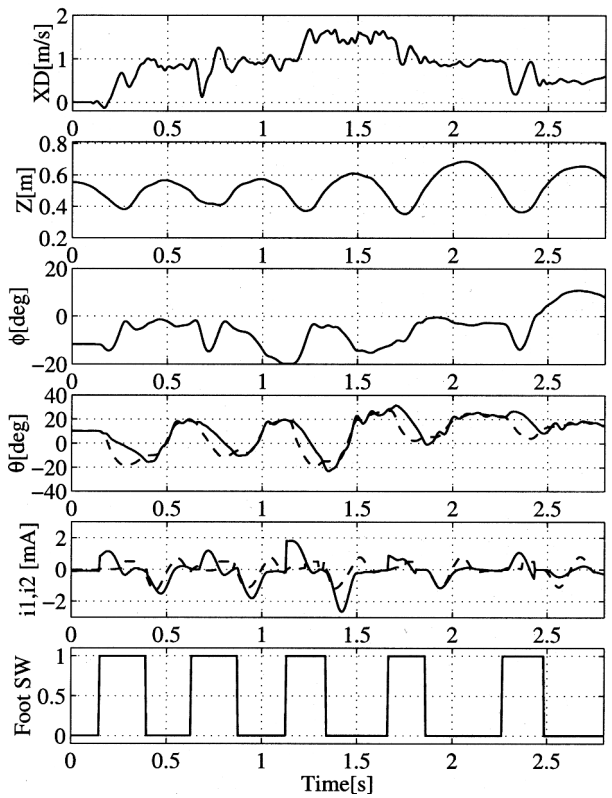

Fig. 24 Experimental results when $\dot{x}_d = 1.5$

the body as Uniroo [**6**] does or by introducing some non-holonomic attitude controls [**23**].

6 CONCLUSIONS

Inspired by biomechanical studies on animal running, a new mechanical model for the hindlimb of a dog was proposed; a one-legged hopping robot, Kenken, was developed. To derive the controller, basic characteristics of the model were examined using a precise dynamic simulator. Although there is room for improvement, especially for the case of high speed, the robot succeeded in planar hopping both in simulation and in experiments. It was found that the leg spring attached as a gastrocnemius or plantaris enables the robot to produce sufficient population force by virtue of an energy transfer from the knee, even if there is no actuator at the angle joint. Figure 25 shows snapshots of a hopping motion at high speed (2 m/s). Although the robot falls after a few steps in this high-speed hopping, it may be the first time that such a realistic and natural gait has been achieved in a machine (not in a computer simulation). Consequently, simulation and experimental results validate the leg model and the controller.

Through this paper, the authors want to emphasize:

1. Investigating characteristic dynamics of the robot is a direct and effective way of determining the controller.
2. Replacing 'massive' actuators with springs and utilizing passive dynamics minimizes the control effort.
3. A biologically inspired mechanical design necessarily yields animal-like dynamic behaviour by dictating the passive dynamics of the model.

However, the authors do not assert that the controller can always be found by a dynamics-based aproach because the model does not always exhibit meaningful dynamics for the desired control task. In this case, how to install passive elements appropriately, such as a spring or damper, into the model arises as an important and interesting problem. Also, the larger the size of the system, the more it becomes difficult to pick up useful characteristic dynamics because it is time consuming. Therefore, some adaptive or learning scheme should be combined with dynamics-based control. This goal is left for future work.

ACKNOWLEDGEMENT

This work is a part of the Grant-in-Aid for the COE Research Project supported by the Japanese Ministry of Education, Science, Sports and Culture.

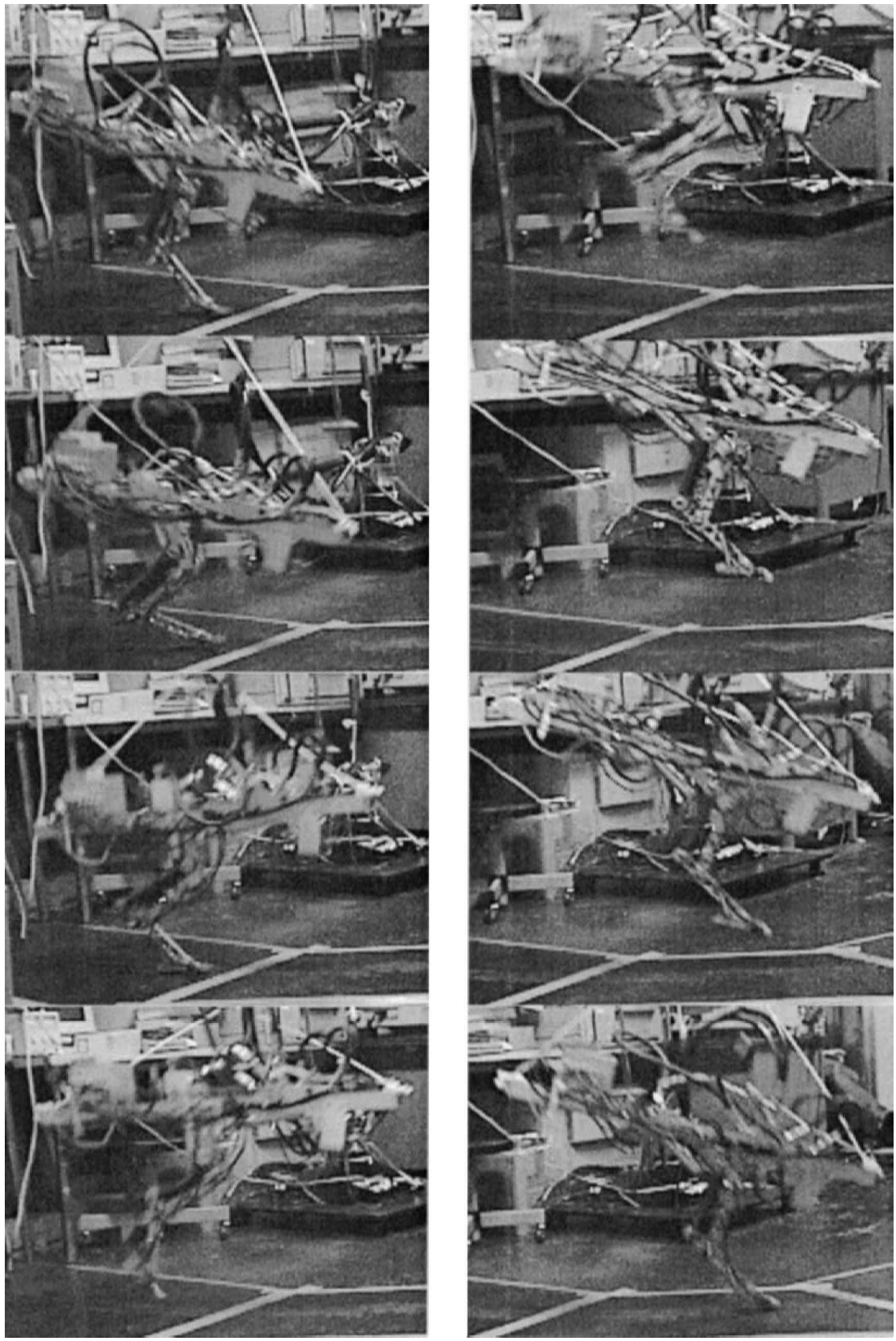

Fig. 25 Snapshots of Kenken hopping for one stride

REFERENCES

1 **Raibert, M. H.** *Legged Robots That Balance*, 1985 (MIT Press, Boston, Massachusetts).
2 **Ahmadi, M.** and **Buehler, M.** The ARL Monopod II running robot: control and energetics. In Proceedings of the IEEE International Conference on *Robotics and Automation*, 1999, pp. 1689–1694.
3 **Ahmadi, M.** and **Buehler, M.** Stable control of a simulated one-legged running robot with hip and leg compliance. *IEEE Trans. Robotics and Automn*, 1997, **13**(1), 96–104.
4 **Saranli, U., Schwind, W. J.** and **Koditschek, D. E.** Toward the control of a multi-jointed, monopod runner. In Proceedings of the IEEE International Conference on *Robotics and Automation*, 1998, pp. 2676–2682.
5 **Lee, W.** and **Raibert, M. H.** Control of hoof rolling in an articulated leg. In Proceedings of the IEEE International Conference on *Robotics and Automation*, 1991, pp. 1386–1391.
6 **Zeglin, G. J.** Uniroo: a one-legged dynamic hopping robot. BS thesis, Department of Mechanical Engineering, MIT, Boston, Massachusetts, 1991.
7 **Hyon, S. H.** and **Mita, T.** Development of a biologically inspired hopping robot—Kenken. In Proceedings of the IEEE International Conference on *Robotics and Automation*, 2002, pp. 3984–3991.
8 **Alexander, R. M.** *Elastic Mechanisms in Animal Movement*, 1988 (Cambridge University Press).
9 **Pennisi, E.** A new view of how leg muscles operate on the run. *Science*, 1997, **275**(21), 1067.
10 **Alexander, R. M.** The maximum forces exerted by animals. *J. Expl Biol.*, 1985, **115**, 231–238.
11 **McMahon, T. A.** and **Cheng, G. C.** The mechanics of running: how does stiffness couple with speed? *J. Biomechanics*, 1990, **23**(Suppl. 1), 65–78.
12 **Farley, C. T., Glasheen, J.** and **McMahon, T. A.** Running springs: speed and animal size. *J. Expl Biol.*, 1993, **185**, 71–86.
13 **McGeer, T.** Passive walking with knees. In Proceedings of the IEEE International Conference on *Robotics and Automation*, 1990, pp. 1640–1645.
14 **Pratt, J.** and **Pratt, G.** Intuitive control of a planar bipedal walking robot. In Proceedings of the IEEE International Conference on *Robotics and Automation*, 1998, pp. 2014–2021.
15 **Prilutsky, B. I., Herzog, W.** and **Leonard, T.** Transfer of mechanical energy between ankle and knee joints by gastrocnemius and plantaris muscles during cat locomotion. *J. Biomechanics*, 1996, **29**(4), 391–403.
16 **Haug, E. J.** *Computer-Aided Kinematics and Dynamics of Mechanical Systems*, 1989 (Allyn and Bacon, Boston, Massachusetts).
17 **Haug, E. J.,** *et al.* Dynamics of mechanical systems with Coulomb friction, stiction, impact and constraint addition–deletion I–III. *Mech. Mach. Theory*, 1986, **21**(5), 401–425.
18 **Alleyne, A.** and **Liu, R.** Nonlinear force/pressure tracking of an electro hydraulic actuator. *Trans. ASME, J. Dynamic Systems, Measmt Control*, 2000, **122**(1), 232–237.
19 **Robinson, D. W.** and **Pratt, G.** Force controllable hydroelastic actuator. In Proceedings of the IEEE International Conference on *Robotics and Automation*, 2000, pp. 1320–1327.
20 *Moog Catalogue, Type 30 Flow Control Servovalves*, Aerospace Group, Moog, Inc. (latest information: http://www.servovalve.com).
21 **Merrit, H. E.** *Hydraulic Control Systems*, 1967 (John Wiley, New York).
22 **Miura, H.** and **Shimoyama, I.** Dynamic walk of a biped. *Int. J. Robotics Res.*, 1984, **3**, 60–74.
23 **Mita, T., Hyon, S. H.** and **Nam, T. K.** Analytical time optimal control solution for a two link planar acrobat with initial angular momentum. *IEEE Trans. Robotics and Automn*, 2001, **17**(3), 361–366.